ACS OMEGA

Open Access

http://pubs.acs.org/journal/acsodf

Article

ENO1/Hsp70 Interaction Domains: In Silico and In Vitro Insight for a Putative Therapeutic Target in Cancer

Maria Rita Gulotta,[†] Ugo Perricone,[†] Patrizia Rubino, Angela Bonura, Salvatore Feo, Agata Giallongo,* and Giovanni Perconti*

Cite This: *ACS Omega* 2025, 10, 5036−5046

Read Online

ACCESS | Metrics & More | Article Recommendations | Supporting Information

ABSTRACT: Alpha-enolase (ENO1) is a multifunctional protein with oncogenic roles. First described as a glycolytic enzyme, the protein performs different functions according to its cellular localization, post-translational modifications, and binding partners. Cell surface-localized ENO1 serves as a plasminogen-binding receptor, and it has been detected in several cell types, including various tumor cells. The plasminogen system plays a crucial role in pathological events, such as tumor cell invasion and metastasis. We have previously demonstrated that the interaction of ENO1 with the multifunctional chaperone Hsp70 increases its surface localization and the migratory and invasive capacity of breast cancer cells, thus representing a novel potential target to counteract the metastatic potential of tumors. Here, we have used computational approaches to map the putative binding region of ENO1 to Hsp70 and predict the key anchoring amino acids, also called hot spots. *In vitro* coimmunoprecipitation experiments were then used to validate the *in silico* prediction of the protein−protein interaction. This work outcome will be further used as a guide for the design of potential ENO1/HSP70 inhibitors.

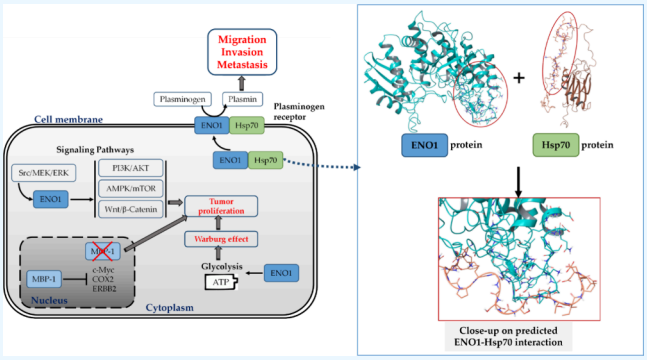

1. INTRODUCTION

Alpha-enolase (ENO1) is a glycolytic enzyme that reacts with 2-phosphoglycerate to form phosphoenolpyruvate in both aerobic and anaerobic glycolysis. ENO1 enzymatic activity has been known since the '30s,[1] but more recent studies have demonstrated that ENO1, in addition to being a cytoplasmic glycolytic enzyme, is a moonlighting protein that participates in a variety of key cellular activities, depending primarily on different cellular localizations. Moonlighting proteins belong to a class of multifunctional proteins that perform fully unrelated cellular functions within one polypeptide chain. As a moonlighting protein, ENO1 supports the ability to coordinate and, in part, control multiple cellular functions, which are frequently altered when the protein is overexpressed or deregulated.[2,3]

ENO1 is commonly overexpressed across a wide range of human tumors and is regarded as a significant cancer biomarker with substantial prognostic and diagnostic potential.[2] For instance, in breast cancer, ENO1 overexpression correlates with larger tumor size and poor nodal status;[4] in lung carcinoma, heightened levels of ENO1 protein are linked to unfavorable clinical outcomes;[5] in the context of pancreatic malignancies, the ENO1 expression level is positively associated with clinical stage, lymph node metastasis, and negative prognosis.[6] In cancer cells, ENO1 overexpression promotes oncogenic events such as the metabolic reprogramming of the cells, activation of signaling pathways, resistance to chemotherapy, regulation of proliferation, apoptosis, and migration.[2,3] It is well-known that altered glucose metabolism is one of the preeminent types of metabolic reprogramming in tumor cells, which adopt the glycolytic pathway for their energy sources instead of the more efficient mitochondrial oxidative phosphorylation pathway (Warburg effect). ENO1 is a key enzyme in the control of glycolysis and energy production, and its overexpression helps to sustain the Warburg effect in cancer cells.[2] In gastric cancer, it has been demonstrated that ENO1 overexpression can be induced through the activation of the Src and MEK/ERK signaling pathways.[7] In addition, overexpressed ENO1 regulates multiple intracellular signaling pathways that control cell proliferation, migration, and apoptosis. It has been shown that ENO1 is a positive regulator of the PI3K/AKT,[8] AMPK/mTOR,[9,10] and Wnt/β-catenin pathways[11] through mechanisms that remain largely unknown, including the modulation of the

Received: November 28, 2024
Revised: January 14, 2025
Accepted: January 22, 2025
Published: January 30, 2025

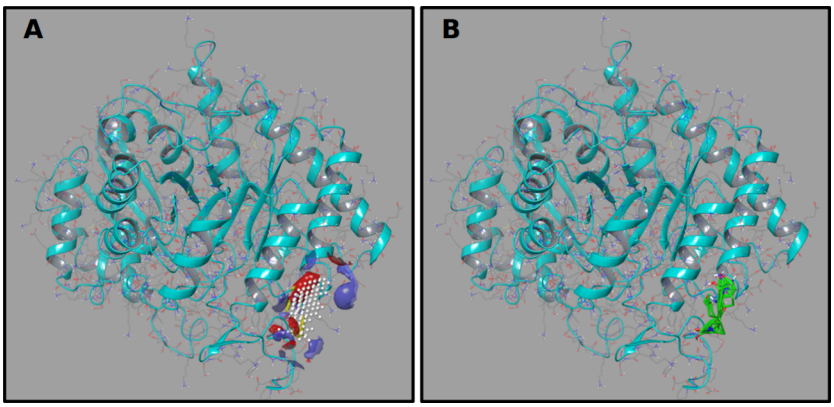

Figure 1. Predicted ENO1 region that putatively interacts with a protein partner. (A) SiteMap-predicted binding site region defined by white site points. Red-colored areas highlight hydrogen-bond acceptor groups; blue-colored areas are for hydrogen-bond donor groups; and yellow-colored portions stand for hydrophobic groups. (B) FTMap-predicted binding site region defined by green molecular probes.

phosphorylation status of upstream regulatory proteins like FAK or AMPKα1 kinases.[8,10]

Other cellular functions are supported by MBP-1 (c-Myc promoter-binding protein 1), an alternative translated form of ENO1 that lacks the first 96 amino acids. Unlike full-length ENO1, MBP-1 is a mainly nuclear protein acting as a transcriptional repressor that regulates the expression of oncogenes, including c-Myc, COX2, and ERBB2.[12−17]

ENO1 is also expressed on the cell surface of a wide variety of cell types, including immune and neuronal cells as well as several pathogenic microorganisms.[2,3,18−22] On the cell surface, ENO1 acts as a plasminogen receptor and, by inducing the release of active plasmin to the pericellular space, acts as a proteolytic factor stimulating cell migration in inflammatory reactions, infection, and tumor invasion.[23−26]

For instance, monocytes use the degradation of the extracellular matrix mediated by surface ENO1 during their recruitment in inflammatory diseases such as pneumonia and rheumatoid arthritis.[18,19,27,28] Moreover, the surface expression of ENO1 has been reported in different cancers, such as lung, pancreatic, and breast cancer. The overexpression of surface ENO1 was found to be related to lymph node metastasis of breast, pancreatic, head, and neck cancer, as well as oral squamous cell carcinoma.[4,6,29−31]

Cell surface expression, along with overexpression in cancer cells, makes ENO1 a tumor-associated antigen that is easily accessible for immunotherapeutic approaches or other therapeutic treatments.

Despite surface ENO1's established role in regulating cancer cell migration and invasion and its potential as a therapeutic target, its membrane topology and the intracellular mechanisms underlying its surface localization remain largely elusive. Enhanced levels of membrane-bound ENO1 in cancer cells were observed after treatment with certain pro-inflammatory molecules, such as lipopolysaccharide (LPS), transforming growth factor-β1 (TGF-β1), and chemokine ligand 2 (CCL2) as well as with other stimuli promoting tumor progression such as epidermal growth factor (EGF).[32,33]

We have previously identified heat shock protein 70 (Hsp70), the product of the HSPA1A gene, as an additional ENO1-interacting protein and demonstrated this chaperone's functional involvement in ENO1 surface localization and, consequently, in cell invasiveness, whether in normal or *in vitro* stimulated conditions.[33] In normal physiological conditions, Hsp70 functions as a molecular chaperone and shields cells from potentially lethal damage induced by stress, ensuring the proper folding of newly synthesized peptides, as well as the sorting of proteins to the correct subcellular compartments, and the assembling of protein complexes.[34] Many studies have shown that Hsp70, like ENO1, is a multifunctional protein that is overexpressed in numerous human cancers. Overexpressed Hsp70 is present mainly in the cytosol but also on the plasma membrane in a tumor-specific manner, playing important roles such as escaping apoptosis and promoting angiogenesis, invasion, treatment resistance, and metastasis formation.[34] Hsp70 affects a wide range of cancer cell behaviors through the deregulation of multiple cancer-related signaling pathways, such as the RTKs-RAS-RAF-MEK-ERK pathway and the PI3K/AKT/mTOR pathway.[35] In addition, Hsp70 hinders the anticancer immune responses, thereby promoting the survival of malignant cells, a function that makes it a promising target for the development of anticancer drugs.[36] ENO1 and Hsp70 have been extremely well-conserved during evolution; both proteins individually play key roles in tumor biology, and their interaction on the cell surface adds a further dimension to their multifunctionality.

In the present study, we have investigated the ENO1-Hsp70 molecular recognition pattern by combining different computational approaches with coimmunoprecipitation experiments, using ENO1 and Hsp70 deletion mutants, to validate computational insights and guide the exploration of ENO1-Hsp70 interactions. This newly investigated protein−protein interaction may represent a viable anticancer target, and the structural information we have gleaned may be useful for the design of specific protein−protein interaction inhibitors as potential antimetastatic agents.

2. RESULTS

2.1. Hsp70-Binding Domain Is Localized to an Internal Region of ENO1. The interaction of the multifunctional protein Hsp70 with ENO1 protein and the relevance of the role of ENO1 in driving pathological conditions, including tumor invasion and metastasis formation, prompted us to characterize its interaction with Hsp70. Therefore, in the attempt to determine which ENO1 region might be responsible for contacting the Hsp70 protein, we coupled computational and experimental ENO1 surface exploration. For the *in silico* analysis, we used SiteMap,[37,38] a tool designed to identify and characterize potential binding sites according to

https://doi.org/10.1021/acsomega.4c10808
ACS Omega 2025, 10, 5036−5046

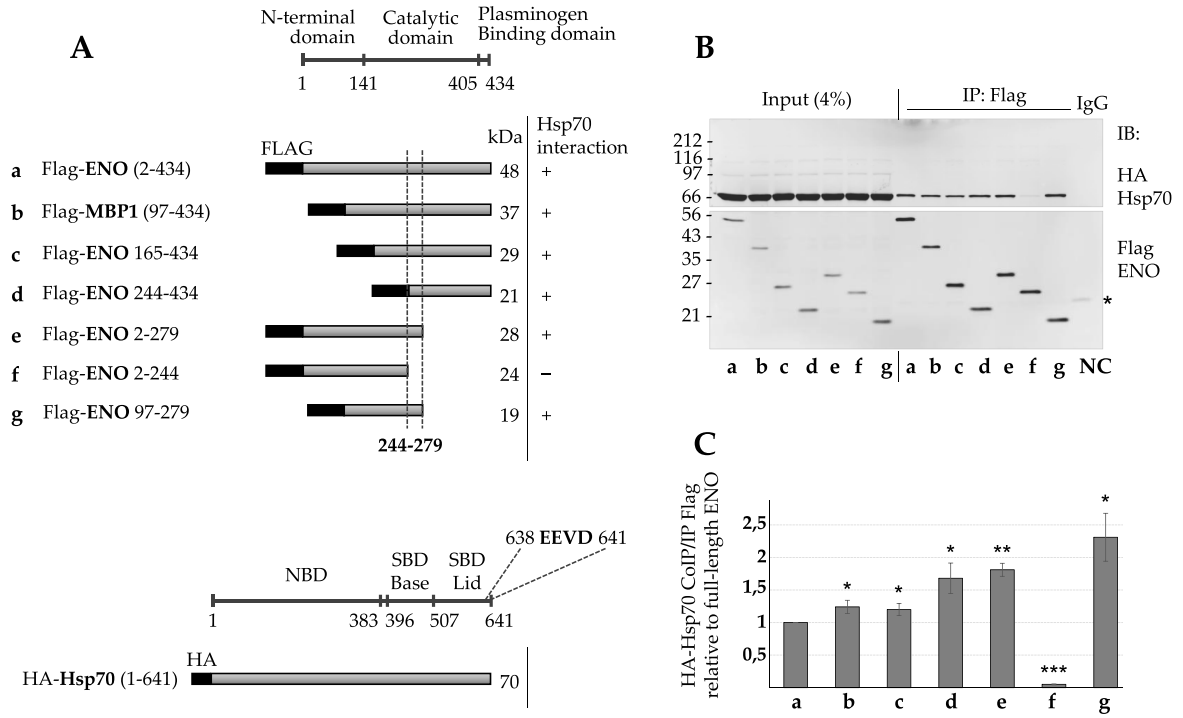

Figure 2. Mapping of the ENO1 domain involved in interaction with Hsp70. (A) Schematic representation of the flag-tagged ENO1 (a) and deletion mutants (b−g) used in coimmunoprecipitation experiments with the full-length HA-tagged Hsp70 construct (below). ENO1 and Hsp70 functional domains are shown. The first and last amino acid and molecular weight (kDa) of each mutant are indicated. (B) Cell lysates from HEK 293T cotransfected with HA-tagged full-length Hsp70 and flag-tagged full-length ENO1 (a) or deletion mutants (b−g) were immunoprecipitated with anti-Flag antibody or a preimmune isotype-matched antibody (IgG; NC stands for negative control) and analyzed by immunoblotting (IB) with the indicated antibodies (anti-HA in the top panel; anti-Flag in the bottom panel). HA-tagged Hsp70 band size was 70 kDa and flag-tagged ENO mutant band sizes ranged from 20 to 55 kDa. Asterisk indicates bands corresponding to immunoglobulin light chains. Full-length blots are presented in Figure S3. (C) Immunoprecipitated and coimmunoprecipitated proteins were quantified by densitometric analysis, and coprecipitated Hsp70 was normalized with respect to the corresponding precipitated ENO polypeptide (a−-g). Input represents 4% of the cell extract used for each IP sample. Results are expressed relative to the coprecipitated Hsp70 obtained with the precipitated full-length ENO (a), set at 1. Error bars represent standard deviation of three independent experiments, and p values ($^*P < 0.05$, $^{**}P < 0.01$, $^{***}P < 0.001$) indicate statistical significance.

some parameters, such as site size and relative extent of solvent exposure as main criteria, and also tightness of the site and hydrophobic and hydrophilic character of the site. According to the literature,[38] SiteMap has been shown to report a good success rate in top-ranking potential binding sites, even for shallow sites involved in protein−protein interactions. However, in order to get a more comprehensive study, another computational tool, FTMap, was used.[39] This tool employs small molecular probes encompassing different sizes, shapes, and polarities to map a protein surface, finding the most energetically favorable protein regions accommodating different probes. Then, the highest is the number and type of probes binding a protein region, and the highest is the probability that the area is a proper binding site. Therefore, the 3D structure of ENO1 protein was retrieved from the Protein Data Bank,[40] according to the best resolution,[26,41] and both tools were set to detect potential binding hotspots for protein−protein interactions. Comparing the results, interestingly both SiteMap and FTMap shared some ENO1 predicted binding sites. However, we decided to focus our attention on a consensus region, that was first-ranked by SiteMap with both the best SiteScore (>0.80 threshold) and DScore (>0.98 threshold as a druggable site). This predicted region includes amino acids from positions 162 to 282, as depicted in Figure 1.

In parallel, the experimental analysis was performed using expression plasmids encoding flag-tagged full-length ENO1 or deletion mutants, as illustrated in Figure 2. The plasmids were individually cotransfected with a vector expressing full-length HA-tagged Hsp70 into human HEK 293T cells. At 48 h post-transfection, aliquots of the total cell lysates were subjected to Western blot analysis using anti-HA and anti-Flag antibodies to check protein expression levels (input in Figure 2B). The protein extracts were immunoprecipitated using anti-Flag or control IgG antibody (IgG in Figure 2B), and coimmunoprecipitated Hsp70 protein was detected by Western blot analysis with anti-HA antibody. No ENO1 coprecipitation was observed when lysates from cells singly expressing HA-tagged Hsp70 were incubated with anti-Flag antibodies, showing the specificity of the interaction with flag-tagged ENO1 and the absence of antibody cross-reactivity (Figure S1). The intensities of the bands were quantified by densitometry, and each coimmunoprecipitated protein signal was normalized against the corresponding immunoprecipitation signal (CoIP/IP). The deletion of the internal region between residues 244 and 279 resulted in the elimination of the interaction with Hsp70, indicating that this portion of ENO1 contains the interaction domain (Figure 2B,C lane f). These experimental findings confirmed the computational predictions that had identified a key ENO1 binding region within amino acids in positions 162 to 282. Furthermore, some of the ENO1 deletion mutants containing the putative interaction domain showed a greater binding capacity for Hsp70 compared to the full-length protein (see mutants d, e, and g), suggesting a different exposure of the amino acid residues involved in the

https://doi.org/10.1021/acsomega.4c10808
ACS Omega 2025, 10, 5036−5046

binding. To validate the findings and exclude any potential interference from the epitopes utilized, the same experiment outlined in Figure 2 was performed using a coding vector yielding the Hsp70 protein fused in frame with a different epitope (Figure S2). This experiment confirms that the observed interactions are independent of the epitopes used, thus validating the reproducibility and robustness of the findings and demonstrating that the results are not affected by any structural influence of the epitopes.

2.2. Analysis of Hsp70 Binding Regions to ENO1: NBD Region Appears Not Interacting with ENO1 Key Residues. The experimental evidence described above provided crucial insights to confirm the region of ENO1 protein responsible for contacting Hsp70 by narrowing the sequence length previously predicted by SiteMap and FTMap to residues in positions 244 to 279. Figure 3 depicts the ENO1 structure, with a close-up of the above-mentioned key amino acids.

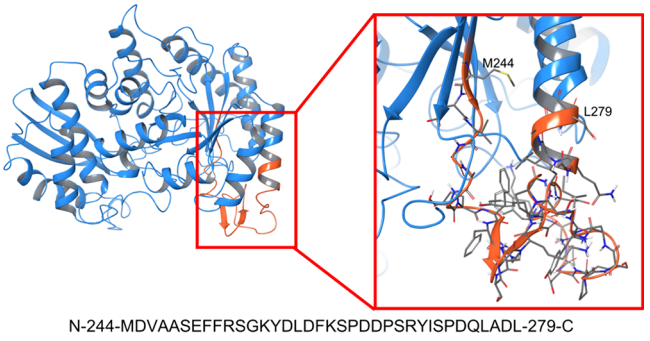

Figure 3. Close-up of the ENO1 region involving residues 244 to 279 (orange portion of the protein structure).

However, the Hsp70 region in contact with ENO1 is still unknown since its complex structure has yet to be solved and deposited in the Protein Data Bank (PDB).[40,41] Therefore, based on the above-reported findings, we pursued a computational exploration to predict and investigate putative ENO1-Hsp70 contact points.

As extensively reported in the literature, Hsp70 consists of an N-terminal, 45 kDa, nucleotide-binding domain (NBD) and a C-terminal, 35 kDa, substrate-binding domain (SBD) bound to each other through a short hydrophobic linker.[42] Unlike the NBD region, the C-terminal portion has been shown to exhibit a certain rate of promiscuity when binding substrates, especially those involving hydrophobic regions, including extended accessible short peptide segments[43,44] and partially folded proteins.[45,46] This promiscuity is responsible for involving Hsp70 in many interactions to maintain the global proteostasis network.[42] In this context, it was crucial to analyze the solvent-exposed side chains of ENO1 amino acids in positions 244 to 279. Indeed, the analysis of the surface highlighted two hydrophobic patches (red circles in Figure 4A) and a partial folding of this region, including loops and a short β-strand (red circles in Figure 4B).

As extensively reported in the literature, the above-mentioned Hsp70 promiscuity has been associated with an intrinsically disordered region (IDR) that, as a matter of fact, falls within the C-terminal portion.[47] Generally, the IDRs are characterized by conformational plasticity due to specific amino acid composition including a low number of bulky hydrophobic residues and, on the contrary, consisting of several amino acids with charged side chains and hydrophilic nature.[48] Furthermore, the IDRs usually contain functional sites, even called molecular recognition features (MoRFs), that are responsible for interactions with structured partner proteins. According to the literature, MoRFs often can undergo a disorder-to-order transition by adopting conformational changes to α-helix, β-strand, or a combination of both.[49] For a more comprehensive analysis, the web-based implementation ANCHOR2[50] was used to analyze the Hsp70 sequence. Indeed, this web tool is able to recognize protein binding regions disordered in isolation and predict whether they can undergo a disorder-to-order transition upon binding. This tool calculates a probability score for each protein residue, where amino acids with values over 0.5 should belong to disordered regions able to interact with protein partners.[51] Thus, the analysis of the resulting graph (see Figure S4) highlighted two key segments in the C-terminus, one from residues 605 to 625 with values between 0.51 and 0.57, and another one in positions 632 to 641 with values between 0.51 and 0.82. These results suggest that these two intrinsically disordered segments should be interested in interactions with protein partners and, as above-mentioned, these segments might exhibit conformational rearrangement upon binding.

2.3. ENO1-Binding Domain Is Localized to the C-Terminal Region of Hsp70. The above-reported consid-

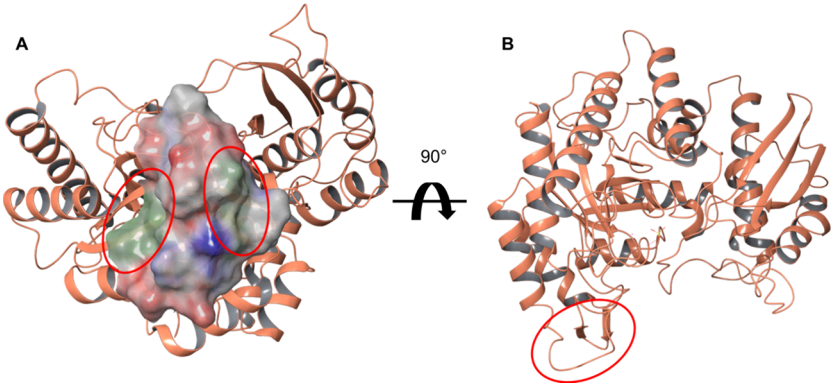

Figure 4. Analysis of ENO1 244 to 279 region. (A) Surface analysis of ENO1 244 to 279 amino acids side chains; green patches are hydrophobic, blue are positive portions, and red are negative areas. (B) The red circle highlights a partial folding of ENO1 portion 244−279, consisting of loops and a short β-strand.

https://doi.org/10.1021/acsomega.4c10808
ACS Omega 2025, 10, 5036−5046

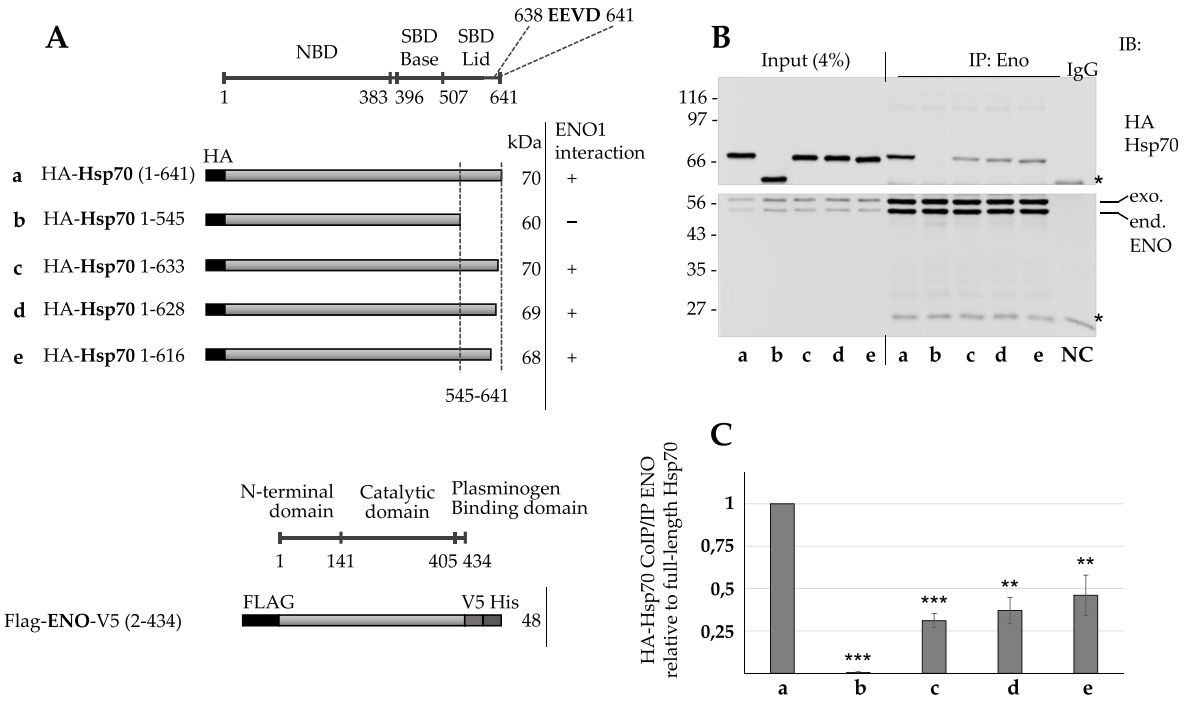

Figure 5. Mapping of the Hsp70 domain involved in the interaction with ENO1. (A) Schematic representation of the full-length HA-tagged Hsp70 (a) and deletion mutants (b−e) used in coimmunoprecipitation experiments with full-length flag-tagged (below) and endogenous ENO1. Hsp70 and ENO1 functional domains are shown. First and last amino acid and molecular weight (kDa) of each mutant are indicated. (B) HEK 293T cells stably expressing full-length Flag-V5-tagged ENO1 were transfected with the HA-tagged full-length Hsp70 (a) or deletion mutants (b−e) shown in A. Cell lysates were immunoprecipitated with monoclonal anti-ENO1 antibody or a preimmune isotype-matched antibody (IgG; NC stands for negative control) and analyzed by immunoblotting with the indicated antibodies (anti-HA in the top panel; anti-ENO1 in the bottom panel). Exogenous (exo.) and endogenous (end.) ENO are indicated. HA-tagged Hsp70 mutant band sizes ranged from 60 to 70 kDa, and endogenous and exogenous ENO bands were 48 and 55 kDa, respectively. Asterisks indicate bands corresponding to immunoglobulin heavy and light chains. Full-length blots are presented in Figure S3. (C) Immunoprecipitated and coimmunoprecipitated proteins were quantified by densitometric analysis, and each coprecipitated full-length Hsp70 or deletion mutant (a−e) was normalized with respect to the corresponding precipitated ENO (exo. and end.). Results are expressed relative to the coprecipitated full-length Hsp70 obtained with the precipitate ENO (a), set at 1. Error bars represent standard deviation of three independent experiments, and p values ($^*P < 0.05$, $^{**}P < 0.01$, $^{***}P < 0.001$) indicate statistical significance.

erations and computational analysis guided the experimental follow-up on the Hsp70 binding region to ENO1. For this purpose, expression plasmids encoding Hsp70 C-terminal deletion mutants were generated as shown in Figure 5A. We previously generated a HEK 293T cell clone stably expressing high levels of recombinant ENO1 protein with a Flag epitope at the N-terminus and a V5 epitope plus six histidine residue tags at the C-terminus (see Figure 5A, lower part).[52] HA-tagged full-length Hsp70 and mutants were transiently expressed in the cells stably expressing full-length multiple-epitope-tagged ENO1 and, at 48 h post-transfection, lysates were subjected to immunoprecipitation with anti ENO1 monoclonal antibody or control IgG antibody (Figure 5B). The immunoprecipitated complexes and aliquots of the total cell lysates (input) were subjected to Western blot using anti-HA or anti-ENO1 antibodies, recognizing exogenous and endogenous ENO1 (exo. and end., in Figure 5B). The intensities of the bands were quantified by densitometry, and each coimmunoprecipitated protein signal was normalized against the corresponding immunoprecipitation signal. The deletion mutant HA-Hsp70 1−545, missing the last 96 amino acid residues, did not show detectable binding to ENO1, confirming the previously reported analysis, i.e., the C-terminal region of the Hsp70 protein contains the sequence required for interaction with ENO1. Furthermore, the C-terminal deletion mutants HA-Hsp70 1−633, 1−628, and 1−616, spanning the last 25 C-terminal residues, showed a comparable residual binding capacity compared with the full-length protein (Figure 5C). Based on these findings, it is likely that Hsp70 residues within positions 545 to 616 should mediate key contacts with ENO1, whereas Hsp70 amino acids from 617 to 641 might lend stability to the protein−protein complex even though they are not responsible and/or essential for ENO1-HSP70 interaction.

These results seem to be in accordance with the computational prediction where the N-terminal portion of Hsp70 did not report contacts with ENO1 key amino acids, thus suggesting that the extreme C-terminal region of Hsp70 contains sequence information required for optimal binding to ENO1.

2.4. Prediction of Putative Contacts between ENO1 Key Amino Acids and the Hsp70 SBD Region. In the attempt to provide a more comprehensive study on the ENO1-Hsp70 interaction, a computational protein−protein docking was run through Glide (Schrödinger) to define a putative protein−protein complex involving the ENO1 region 244−279 and the Hsp70 C-terminal portion. However, the PDB Hsp70 SBD structures lack some portions of the C-terminus, and the absence of the NBD portion might wrongly affect computational docking predictions by generating misleading ENO1-Hsp70 complexes. Thus, a full-length model of the Hsp70 protein was downloaded from the AlphaFold repository[53] and it was employed for the subsequent steps of this work. Thanks to the previous experimental findings, it was possible to define

https://doi.org/10.1021/acsomega.4c10808
ACS Omega 2025, 10, 5036−5046

attraction restraints set on both of the key regions of ENO1 and Hsp70, involving amino acids 244 to 279 and 545 to 616, respectively. The output analysis sheds light on some interesting top-ranked docking poses, where the Hsp70 C-term fits the ENO1 244−279 region. In order to choose the most suitable docking pose, MM-GBSA calculations were run to identify the energetically most favorable docked pose. Thus, pose 17 was selected reporting the lowest $\Delta G_{binding}$ value (−70.28 kcal/mol) (see Figure 6 for the glide docked pose).

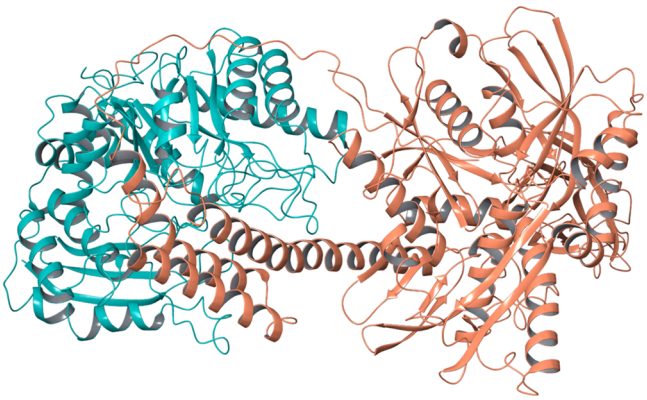

Figure 6. Docking pose of ENO1 (light blue chain) in complex with Hsp70 (orange chain) selected according to MM-GBSA values.

Furthermore, in order to explore the stability of the complex and the frequency of contacts, molecular dynamics (MD) simulations of 200 ns were run in triplicate.

The trajectory stability of the three MD simulations was analyzed through the RMSD plots reported in Table S1. Furthermore, to investigate the relevance of the contacts between ENO1 and Hsp70, the MD frames were then clustered (five clusters for each simulation) according to the RMSD variation. The related cluster centroids were analyzed to retrieve the key contacts between amino acids of both protein partners and, finally, the stability of the observed contacts was analyzed by plotting the occurrence frequency during the entire simulation time. Tables S2−S4 report the plots of the stable contacts between ENO1 and Hsp70 amino acids during the three MD simulations. Finally, Table 1 below lists ENO1 and Hsp70 amino acid key contacts according to stability analysis performed on the three MD simulations. As it can be observed, some amino acids among the experimentally identified residues for both proteins are listed in Table 1; however, the reported contacts seem to have a concerted effect involving also a few amino acids from regions external to the key ones experimentally identified.

Table 1. ENO1 and Hsp70 Are Key Amino Acids Involved in Interactions According to MD Simulation Analysis

ENO1 residues	Hsp70 residues	interaction type
Lys54	Glu588	H-bond + salt bridge
Lys162	Gly132	H-bond + salt bridge
Leu218, Glu219	Gly136	H-bond
Glu250	Arg596	H-bond
Arg253	Asn548	H-bond
Lys262	Glu530, Arg533, Glu534	H-bond + salt bridge
Tyr270	Ser544	H-bond
Asp278	Lys628, Ser631	H-bond + salt bridge
Lys281	Gly621, Gly623	H-bond
Tyr287	Ser633	H-bond
Asp297	Asn604	H-bond
Gln298	Glu600	H-bond
Asp299	Asn604, Ser608, Gln612	H-bond

In light of this computational analysis, in our opinion, the collected data provide crucial insights that may guide future steps of this work. Indeed, predicting the binding mode of Hsp70 to ENO1 and, consequently, identifying the anchoring points on both proteins should allow us to perform a supervised virtual screening campaign to select putative modulators of the ENO1-Hsp70 interaction.

3. DISCUSSION

Upon oncogenic or inflammatory stimulation, the expression of surface ENO1 as a plasminogen receptor increases in tumor cells, enhancing their migratory and invasive potential. Thus, targeting surface ENO1 represents a powerful therapeutic strategy for metastatic cancer treatment. In the highly aggressive pancreatic ductal adenocarcinoma (PDAC), it has been shown that antibodies against surface ENO1 inhibit the plasminogen-dependent invasion *in vitro*, and the formation of lung and bone metastasis *in vivo*.[23,54] Cappello developed a DNA vaccine capable of inducing anti-ENO1 antibody production, thus significantly reducing tumor progression in preclinical models of PDAC.[55,56]

In the past decade, significant research efforts have resulted in the design and development of small-molecule inhibitors of ENO1 to treat cancer as well as inflammatory diseases and other pathological conditions.[57−60] However, none of the small molecules directed against ENO1 have been designed to selectively inhibit the activity of the surface-localized protein. Several studies have shown that ENO1 interacts with protein partners, such as uPA, uPAR, annexin 2, caveolin-1, B7−H3, granulin A, integrins, and cytoskeletal proteins, that seem to contribute to regulating its cell-surface translocation and functioning. These proteins may be part of one or more protein complexes containing ENO1 involved in cell adhesion, migration, and proliferation.[22,32,61]

We have previously established Hsp70 as an additional ENO1 interactor.[33] Although it is commonly known as a cytosolic molecular chaperone, Hsp70, like ENO1, is a multifunctional oncoprotein with different cell localizations, and it is overexpressed in human malignancies.[62] Hsp70 is present on the plasma membrane of a wide variety of solid tumors but not on corresponding normal tissues, and it is involved in the control of important cellular functions such as tumor immunosurveillance.[62] We have already demonstrated the functional involvement of Hsp70 in the ENO1 surface localization, showing that the silencing of Hsp70 expression in cancer cells results in a specific downregulation of the surface ENO1 steady-state level, as well as in the inhibition of EGF- and LPS-mediated ENO1 surface translocation.[33] In this study, we used computational and experimental methods to identify putative key amino acids of the domains responsible for the interaction between ENO1 and Hsp70 proteins. According to our computational mapping on the ENO1 surface and the results obtained from coimmunoprecipitation experiments with a panel of ENO1 deletion mutants, we first determined the domain mediating the interaction with Hsp70 in the ENO1 internal region between residues 244 and 279. Subsequently, multiple computational studies were performed to predict the Hsp70 portion responsible for contacting the established

https://doi.org/10.1021/acsomega.4c10808
ACS Omega 2025, 10, 5036−5046

ENO1 interaction domain. This computational prediction of the Hsp70 binding region to ENO1 was experimentally explored; finally, MD simulations were performed and the analysis of the trajectories shed light on residues from both proteins putatively responsible for the protein−protein complex formation.

To date, a binding motif within the ENO1 sequence, i.e., between amino acid residues 296 and 304 has been identified only for its interaction with caveolin-1.[63] This caveolin binding motif does not overlap with the site we identify here for Hsp70 interaction; however, the two sequences are close to each other in a region of the protein that is not enveloped deep inside the protein core but, in contrast, is well exposed on the surface of the protein (Figure 3). The plasminogen binding activity of ENO1 has been mapped to the extreme C-terminal portion of the protein, but another putative plasminogen binding site has been located at N-250-FFRSGK-256-C.[26] The Hsp70-binding domain identified here could therefore be part of a highly accessible and available region of the ENO1 protein that mediates the interaction with different protein partners.

Our data contribute to unraveling the molecular mechanisms that regulate the different activities and localization of the multifunctional proteins ENO1 and Hsp70. In addition, the protein−protein interaction mapped in this study could be considered as a novel therapeutic target for metastatic cancer management, and its molecular definition will provide the basis for the design of specific inhibitors as potential antimetastatic agents.

4. METHODS

4.1. Cell Lines and Culture Conditions. Embryonic Kidney 293T (HEK 293T) from laboratory stocks were originally obtained from American Type Culture Collection (ATCC, Rockville, MD, USA), and 293-T/Flag-Eno-V5 cells, stably expressing the recombinant multiple-epitope-tagged ENO1, have been previously described.[52] Cells were cultured in Dulbecco's modified Eagle medium (DMEM; Sigma-Aldrich) supplemented with 10% heat-inactivated fetal bovine serum (FBS; Sigma-Aldrich), 4 mM glutamine (Euroclone), 1 mM sodium pyruvate (Sigma−Aldrich), and 100 μg/mL penicillin/streptomycin (Sigma-Aldrich) in a 5% CO_2 atmosphere.

4.2. Plasmid Construction and Transfection. The ENO1 cDNA was obtained by polymerase chain reaction (PCR) amplification using an expression vector coding for the full-length protein[12] as a template and PSA-2/SP6 primers. The PSA-2 primer introduced a HindIII restriction site into PCR-amplified cDNA. pFlag-ENO expression vector was obtained by cloning full-length ENO1 cDNA into the mammalian expression vector pFLAG-CMV-2 (Sigma-Aldrich) using HindIII and XbaI restriction sites. The resulting construct expresses the entire ENO1 protein with a Flag tag at the N terminus. For the construction of Flag-MBP-1, Flag-ENO 165−434, and Flag-ENO 244−434 vectors, the cDNAs were amplified from the pFlag-ENO vector by PCR. The PCR reaction was performed with PSA-97, PSA-165, and PSA-244 as 5′-primers and CMV24 as 3′-primers. The PCR products were HindIII/XbaI digested, and the purified fragments were cloned in the pFLAG-CMV-2 vector digested with the same enzymes. For the construction of the Flag-ENO 2−279 vector, mutagenesis by the quick-change kit (Stratagene, La Jolla, CA, USA) was performed on the Flag-ENO plasmid template changing codon 280 (tyrosine) into a stop codon (TAA). For construction of the Flag-ENO 97−279 vector, mutagenesis was performed on the Flag-MBP1 plasmid template changing codon 280 into a stop codon. For the construction of the Flag-ENO 2−243 vector, the cDNA coding amino acids 2 to 243 of ENO1 was amplified from Flag-ENO 2−279 vector by PCR with Flag ENO1 and Flag Anti 243 primers and inserted into the HindIII/XbaI site of the pFlag-CMV-2 mammalian expression vector. HA-Hsp70 vector, coding for N-terminal HA-tagged full-length Hsp70, was purchased from Sino Biological Inc. (Cat.N. HG11660-NY). For the construction of the HA-Hsp70 1−545 vector, the cDNA coding amino acids 1 to 545 of Hsp70 was amplified from the HA-Hsp70 vector by PCR with sense-HA and antisense-HA1 primers and inserted into the HA-Hsp70 backbone vector double digested by the HindIII/XbaI restriction enzymes and gel-purified. The HA-Hsp70 1−633, 1−628, and 1−616 expression vectors were constructed in the same way as the HA-Hsp70 1−545 using the sense HA and antisense primers HA2, HA3, and HA4, respectively. Myc-Hsp70 vector, coding for N-terminal Myc-tagged full-length Hsp70, was purchased from Sino Biological Inc. (Cat.N. HG11660-NM). All of the construct sequences were confirmed by DNA sequencing analysis. Primers for plasmid construction are listed in the Supporting Information (Table S5). Cells were transfected with the indicated plasmid DNAs using Lipofectamine 2000 reagents (ThermoFisher Scientific) according to the manufacturer's instructions. The generation of stably transfected HEK 293T cells expressing a multiple-epitope-tagged full-length ENO1 was described previously[52].

4.3. Cell Lysis and Coimmunoprecipitation. At 48 h post-transfection, cells were resuspended in lysis buffer (20 mM Tris−HCl pH 7.6, 100 mM NaCl, 1% NonidetP40, 2 mM EDTA, 60 mM Octyl-β-D-glucopyranoside) supplemented with protease and phosphatase inhibitor cocktails (Sigma-Aldrich) incubated on ice for 40 min and cleared by centrifugation at 8000 xg for 10 min at 4 C. Protein content was determined using the Bradford protein assay (Bio-Rad Laboratories). For immunoprecipitation, 100 μg of cell lysates in 200 μL of lysis buffer were incubated for 2 h with 2 μg of either mouse monoclonal anti-FLAG M2 (Sigma-Aldrich, Cat. A2220) or anti ENO1 (Santa Cruz Biotechnology, Cat. sc-100812) monoclonal antibody previously linked to Protein A/G agarose beads (Santa Cruz Biotechnology, Cat. no. sc-2003). The immune complexes were spun down and washed three times with lysis buffer. The specificity of the precipitated immunocomplexes was assessed using IgG isotype controls (Santa Cruz Biotechnology, Cat. SC3877). Bound proteins were eluted in sample buffer for SDS-PAGE supplemented with 5% 2-mercaptoethanol incubating at 100 °C for 5 min.

4.4. Western Blot Analysis. Proteins from cell lysates (input) or from immunopurified protein samples (IP) were separated on 9% or 11% polyacrylamide gels and then transferred onto a nitrocellulose membrane. Membranes were blocked and incubated for 1 h with primary antibody (HA monoclonal antibody, HA-7 clone, Sigma-Aldrich, 1:10000; FLAG M2, Sigma-Aldrich, 1:10000; ENO1 monoclonal antibody, Santa Cruz Biotechnology, 1:1000; Myc mouse monoclonal antibody, 9E10 clone, Santa Cruz Biotechnology, 1:1000), diluted in Blocking Buffer Li-Cor Biosciences, and then washed 3 × 10 min in TBS (137 mM NaCl, 20 mM Tris/HCl, pH 7.6) supplemented with 0.05% Tween-20 (Sigma-Aldrich). Membranes were incubated with secondary antibody conjugated to IRDye 800CW (LI-COR), diluted 1:10000 in

https://doi.org/10.1021/acsomega.4c10808
ACS Omega 2025, 10, 5036−5046

Blocking Reagent (LI-COR, Cat. 927−60001) for 1 h, and then washed 3 × 10 min in TBS with 0.05% Tween-20. Bands were visualized using the Odyssey infrared imaging system (LI-COR Biosciences) according to the manufacturer's instructions.

4.5. Statistical Analyses. All data are presented as means ± standard deviation of at least three experiments. The statistical significance of the results was assessed by paired, one-sided Student's *t* test; statistical differences are presented at probability levels of $*P < 0.05$, $**P < 0.01$, $***P < 0.001$.

4.6. Preparation of the Hsp70 NBD and SBD Regions and the ENO1 Protein for Computational Analysis. The crystal structure of ENO1 protein was retrieved from the Protein Data Bank[40] according to the best resolution (PDB id 3B97[26,41]), while the full-length model of Hsp70 was downloaded from AlphaFold repository.[53] The protein structures were prepared and optimized through the Schrödinger suite (Schrödinger, LLC, New York, NY, software release v2021−3).[64] Known HET groups from the Chemical Component Dictionary were employed to assign bond orders to untemplated residues. Water molecules beyond 5.0 Å from any of the HET groups, including ions, were deleted. Hydrogens were added to the structure, zero-order bonds between metals and nearby atoms were added, and formal charges to metals and neighboring atoms were adjusted. Disulfide bonds were created according to possible geometries. Epik[65,66] was used to generate protonation and metal charge states for the ligands and cofactors at pH 7.4 ± 0.2. Finally, PROPKA[67] was run under pH 7.4 to optimize hydroxyl groups and Asn, Gln, and His states.

4.7. Computational Mapping on the ENO1 Protein Surface. Two computational tools were used to map the ENO1 surface and identify putative binding sites. The first tool was SiteMap.[37,38] For this purpose, the PDB structure 3B97[26,41] previously prepared was used, and to define a putative binding site at least 15 site points were required. Up to 10 sites were reported, and the hydrophobicity of the binding site was defined as more restrictive. The grid used was standard, and the site maps were cropped at 4 Å from the nearest site points. Finally, shallow binding sites were also investigated. According to these settings, two scores were mainly retrieved, the SiteScore and the DScore, according to eqs 1 and 2, respectively.

$$\text{site score} = 0.0733n^{1/2} + 0.6688e - 0.20p \quad (1)$$

$$D\ \text{score} = 0.094n^{1/2} + 0.60e - 0.324p \quad (2)$$

where n stands for the number of site points included in the predicted site, capped at 100, e is the degree of enclosure of the site, and p is the hydrophilic score calculated for the predicted site.

4.8. Protein−Protein Docking between ENO1 and Hsp70. To predict the putative complex structure of the ENO1-Hsp70 NBD region, the prepared structures of both proteins were used to run a protein−protein docking. For this purpose, chain A of PDB 3B97[41] was considered, while the other chains were neglected and deleted. For this purpose, BioLuminate from the Schrödinger suite (BioLuminate, Schrödinger, New York, NY, software release v2021−3) was used. ENO1 was defined as the receptor and HSP70 as the ligand. A standard search algorithm was set based on up to 70,000 ligand rotations to probe, and the 1000 top-scoring rotations were then clustered based on the binding site RMSD. The maximum number of docking structures to return was set by 30 for each solution. Finally, attractive restraints were included on ENO1 amino acids 244−279 and Hsp70 residues 545−616, and the output structures were refined.

4.9. Molecular Dynamics Simulation of ENO1 in Complex with the Hsp70 NBD Region in Triplicate. In this work, three MD simulations of 200 ns per each were performed using Desmond[68] on the complex ENO1-Hsp70 NBD region retrieved Schrödinger docking results. For all three trajectories, MD simulations were computed by applying the same settings below described. The systems were created using TIP3P[69] as a solvent model, an orthorhombic shape box (10 Å as side distance), and an OLPS4 force field.[69] The resulting systems were neutralized by adding Na^+ ions. The thermostat method employed was the Nosé−Hoover chain with a relaxation time of 1.0 ps and a temperature of 310 K. The barostat method applied was Martyna−Tobias−Krein, with a relaxation time of 2.0 ps and an isotropic coupling style. The time step for numerical integration was 2.0 fs for bonded interactions, 2.0 fs for nonbonded-near (van der Waals and short-range electrostatic interactions), and 6.0 fs for nonbonded-far (long-range electrostatic interactions). For Coulombic interactions, a cutoff radius of 9.0 Å was tuned as a short-range method. Pressure and temperature were set at 1.01325 bar and 310 K, respectively. Finally, the systems were relaxed before beginning the simulations according to the following steps: (1) a minimization with the solute restrained and another minimization without restraints; (2) 12 ps in the NVT ensemble with a Berendsen thermostat, temperature of 10 K, a fast temperature relaxation constant, velocity resampling every 1 ps, and non-hydrogen solute atoms restrained; (3) 12 ps in the NPT ensemble in a Berendsen thermostat and barostat, temperature equal to 10 K and a pressure of 1 atm, a fast temperature relaxation constant, a slow pressure relaxation constant, velocity resampling every 1 ps, and nonhydrogen solute atoms restrained; (4) 24 ps in the NPT ensemble with a Berendsen thermostat and barostat, temperature of 300 K and a pressure of 1 atm, a fast temperature relaxation constant, a slow pressure relaxation constant, velocity resampling every 1 ps, and non-hydrogen solute atoms restrained; (5) a final step of 24 ps of relaxation in the NPT ensemble using a Berendsen thermostat and barostat, a temperature of 300 K and a pressure of 1 atm, a fast temperature relaxation constant, and a normal pressure relaxation constant.

4.10. MD Trajectory Frame Clustering. The trajectories retrieved from the MD simulations performed on the ENO1-Hsp70 complexes were used to perform clustering. For the MD simulations, the same settings herein reported were employed. The RMSD matrix calculation was set using the protein backbone as a reference, the frequency of frames analysis was set to 10, and the hierarchical cluster linkage method was average. Finally, for both MD trajectories, five clusters were generated.

■ ASSOCIATED CONTENT

Data Availability Statement

All data generated or analyzed during this study are included in this published article and its Supporting Information files.

Supporting Information

The Supporting Information is available free of charge at https://pubs.acs.org/doi/10.1021/acsomega.4c10808.

https://doi.org/10.1021/acsomega.4c10808
ACS Omega 2025, 10, 5036−5046

Absence of cross-reactivity of anti-Flag monoclonal antibody with HA-Hsp70 protein (Figure S1); deletion of the ENO1 internal region 244−279 abolishes the interaction with Hsp70 regardless of the epitopes used (Figure S2); images of the full blots, with visible edges, that are shown cropped in Figures 2 and 6 (Figure S3); ANCHOR2 graph on Hsp70 sequence (Figure S4); RMSD plots of three MD simulations performed on ENO1 protein complexed with Hsp70 protein retrieved from protein−protein docking (Table S1); plots of occurrence frequency of stable contacts between ENO1 and Hsp70 proteins during the first MD simulation (Table S2); plots of occurrence frequency of stable contacts between ENO1 and Hsp70 proteins during the second MD simulation (Table S3); plots of occurrence frequency of stable contacts between ENO1 and Hsp70 proteins during the third MD simulation (Table S4); primers used for expression plasmid construction (Table S5) (PDF)

AUTHOR INFORMATION

Corresponding Authors

Agata Giallongo − *Institute of Biomedical Research and Innovation (IRIB), National Research Council (CNR), Palermo 90146, Italy*; Phone: +39 091 6809543; Email: agata.giallongo@cnr.it

Giovanni Perconti − *Institute of Translational Pharmacology (IFT), National Research Council (CNR), Palermo 90146, Italy; Institute of Biomedical Research and Innovation (IRIB), National Research Council (CNR), Palermo 90146, Italy*; orcid.org/0009-0009-9527-2917; Phone: +39 091 6809543; Email: giovanni.perconti@ift.cnr.it

Authors

Maria Rita Gulotta − *Molecular Informatics Group, Fondazione Ri.MED, Palermo 90129, Italy*

Ugo Perricone − *Molecular Informatics Group, Fondazione Ri.MED, Palermo 90129, Italy*; orcid.org/0000-0002-2181-2468

Patrizia Rubino − *Institute of Translational Pharmacology (IFT), National Research Council (CNR), Palermo 90146, Italy*

Angela Bonura − *Institute of Translational Pharmacology (IFT), National Research Council (CNR), Palermo 90146, Italy*

Salvatore Feo − *Department of Biological Chemical and Pharmaceutical Sciences and Technologies (STEBICEF), University of Palermo, Palermo 90128, Italy*

Complete contact information is available at: https://pubs.acs.org/10.1021/acsomega.4c10808

Author Contributions

†M.R.G. and U.P. contributed equally to this work. G.P. and A.G. conceived and supervised the study, designed experiments, and analyzed the data; U.P. and M.R.G. performed all the computational analysis; G.P. and P.R. performed experiments; S.F. provided some of the plasmid vectors for the immunoprecipitation assay; G.P., U.P., and A.G. wrote the manuscript; S.F. and A.B. contributed to the manuscript revision. All authors approved the submitted version.

Notes

The authors declare no competing financial interest.

ACKNOWLEDGMENTS

This work was supported by the Regione Siciliana, through the PO FESR action 1.1.5 (project OBIND N.086202000366). The authors gratefully acknowledge Richard Burket for the professional English language editing of the manuscript.

REFERENCES

(1) Cummins, H. *Biochem. Z.* **1934**, *273*, 273.

(2) Li, Y.; Liu, L.; Li, B. Role of ENO1 and its targeted therapy in tumors. *J. Transl Med.* **2024**, *14;22* (1), 1025.

(3) Didiasova, M.; Schaefer, L.; Wygrecka, M. When Place Matters: Shuttling of Enolase-1 Across Cellular Compartments. *Front Cell Dev Biol.* **2019**, *7*, 61.

(4) Tu, S. H.; et al. Increased expression of enolase alpha in human breast cancer confers tamoxifen resistance in human breast cancer cells. *Breast Cancer Res. Treat.* **2010**, *121* (3), 539−53.

(5) Zhang, L.; Wang, H.; Dong, X. Diagnostic value of α-enolase expression and serum α-enolase autoantibody levels in lung cancer. *J. Bras Pneumol.* **2018**, *44* (1), 18−23.

(6) Yin, H.; Wang, L.; Liu, H. L. ENO1 overexpression in pancreatic cancer patients and its clinical and diagnostic significance. *Gastroenterol Res. Pract.* **2018**, *2018*, 1.

(7) Chen, S.; Duan, G.; Zhang, R.; Fan, Q. Helicobacter pylori cytotoxin-associated gene A protein upregulates α-enolase expression via Src/MEK/ERK pathway: implication for progression of gastric cancer. *Int. J. Oncol.* **2014**, *45* (2), 764−70.

(8) Fu, Q. F.; Liu, Y.; Fan, Y.; Hua, S. N.; Qu, H. Y.; Dong, S. W.; Li, R. L.; Zhao, M. Y.; Zhen, Y.; Yu, X. L.; Chen, Y. Y.; Luo, R. C.; Li, R.; Li, L. B.; Deng, X. J.; Fang, W. Y.; Liu, Z.; Song, X.; et al. Alpha-enolase promotes cell glycolysis, growth, migration, and invasion in non-small cell lung cancer through FAK-mediated PI3K/AKT pathway. *J. Hematol Oncol.* **2015**, *8*, 22.

(9) Zhan, P.; et al. α-enolase promotes tumorigenesis and metastasis via regulating AMPK/mTOR pathway in colorectal cancer. *Mol. Carcinog.* **2017**, *56* (5), 1427−1437.

(10) Dai, J.; Zhou, Q.; Chen, J.; Rexius-Hall, M. L.; Rehman, J.; Zhou, G.; et al. Alpha-enolase regulates the malignant phenotype of pulmonary artery smooth muscle cells via the AMPK-Akt pathway. *Nat. Commun.* **2018**, *9* (1), 3850.

(11) Ji, M.; et al. Up-regulated ENO1 promotes the bladder cancer cell growth and proliferation via regulating β-catenin. *Biosci Rep.* **2019**, *39* (9), No. BSR20190503.

(12) Feo, S.; Arcuri, D.; Piddini, E.; Passantino, R.; Giallongo, A. ENO1 gene product binds to the c-myc promoter and acts as a transcriptional repressor: relationship with Myc promoter-binding protein 1 (MBP-1). *FEBS Lett.* **2000**, *473* (1), 47−52.

(13) Subramanian, A.; Miller, D. M. Structural analysis of ENO1. Mapping the functional domains involved in down-regulation of the c-myc protooncogene. *J. Biol. Chem.* **2000**, *275* (8), 5958−65.

(14) Hsu, K. W.; et al. MBP-1 suppresses growth and metastasis of gastric cancer cells through COX-2. *Mol. Biol. Cell* **2009**, *20* (24), 5127−37.

(15) Contino, F.; Mazzarella, C.; Ferro, A.; Lo Presti, M.; Roz, E.; Lupo, C.; Perconti, G.; Giallongo, A.; Feo, S.; et al. Negative transcriptional control of ERBB2 gene by MBP-1 and HDAC1: Diagnostic implications in breast cancer. *BMC Cancer.* **2013**, *13*, 81.

(16) Lo Presti, M.; et al. Myc promoter-binding protein-1 (MBP-1) is a novel potential prognostic marker in invasive ductal breast carcinoma. *PLoS One* **2010**, *5* (9), No. e12961.

(17) Perconti, G.; et al. The kelch protein NS1-BP interacts with alpha-enolase/MBP-1 and is involved in c-Myc gene transcriptional control. *Biochim. Biophys. Acta* **2007**, *1773* (12), 1774−85.

(18) Wygrecka, M.; et al. Enolase-1 promotes plasminogen-mediated recruitment of monocytes to the acutely inflamed lung. *Blood* **2009**, *113* (22), 5588−98.

(19) Bae, S.; et al. Alpha enolase expressed on the surfaces of monocytes and macrophages induces robust synovial inflammation in rheumatoid arthritis. *J. Immunol.* **2012**, *189* (1), 365−72.

(20) Haque, A.; Polcyn, R.; Matzelle, D.; Banik, N. L. New Insights into the Role of Neuron-Specific Enolase in Neuro-Inflammation, Neurodegeneration and Neuroprotection. *Brain Sci.* **2018**, *8* (2), 33.
(21) Satala, D.; Bednarek, A.; Kozik, A.; Rapala-Kozik, M.; Karkowska-Kuleta, J. The Recruitment and Activation of Plasminogen by Bacteria-The Involvement in Chronic Infection Development. *Int. J. Mol. Sci.* **2023**, *24* (13), 10436.
(22) Almaguel, F. A.; Sanchez, T. W.; Ortiz-Hernandez, G. L.; Casiano, C. A. ENO1: Emerging Tumor-Associated Antigen, Cancer Biomarker, and Oncotherapeutic Target. *Front Genet.* **2021**, *11*, No. 614726.
(23) Hsiao, K. C.; et al. Surface α-enolase promotes extracellular matrix degradation and tumor metastasis and represents a new therapeutic target. *PLoS One* **2013**, *8* (7), No. e69354.
(24) Miles, L. A.; et al. Role of cell-surface lysines in plasminogen binding to cells: identification of alpha-enolase as a candidate plasminogen receptor. *Biochemistry* **1991**, *30* (6), 1682−91.
(25) Redlitz, A.; Fowler, B. J.; Plow, E. F.; Miles, L. A. The role of an enolase-related molecule in plasminogen binding to cells. *Eur. J. Biochem.* **1995**, *227* (1−2), 407−15.
(26) Kang, H. J.; Jung, S. K.; Kim, S. J.; Chung, S. J. Structure of human alpha-enolase (hENO1), a multifunctional glycolytic enzyme. *Acta Crystallogr. D Biol. Crystallogr.* **2008**, *64* (Pt 6), 651−657.
(27) Chiangjong, W.; Thongboonkerd, V. Calcium oxalate crystals increased enolase-1 secretion from renal tubular cells that subsequently enhanced crystal and monocyte invasion through renal interstitium. *Sci. Rep.* **2016**, *6*, 24064.
(28) Díaz-Ramos, Á.; Roig-Borrellas, A.; García-Melero, A.; López-Alemany, R. ENO1, a multifunctional protein: its role on pathophysiological situations. *J. Biomed Biotechnol.* **2012**, 1.
(29) Tsai, S. T.; et al. ENO1, a potential prognostic head and neck cancer marker, promotes transformation partly via chemokine CCL20 induction. *Eur. J. Cancer.* **2010**, *46* (9), 1712−23.
(30) Wu, W.; et al. Identification and validation of metastasis-associated proteins in head and neck cancer cell lines by two-dimensional electrophoresis and mass spectrometry. *Clin Exp Metastasis.* **2002**, *19* (4), 319−26.
(31) Wang, J.; et al. ENO1 Binds to ApoC3 and Impairs the Proliferation of T Cells via IL-8/STAT3 Pathway in OSCC. *Int. J. Mol. Sci.* **2022**, *23* (21), 12777.
(32) Didiasova, M.; et al. STIM1/ORAI1-mediated Ca2+ Influx Regulates Enolase-1 Exteriorization. *J. Biol. Chem.* **2015**, *290* (19), 11983−99.
(33) Perconti, G.; Maranto, C.; Romancino, D. P.; Rubino, P.; Feo, S.; Bongiovanni, A.; Giallongo, A.; et al. Pro-invasive stimuli and the interacting protein Hsp70 favour the route of alpha-enolase to the cell surface. *Sci. Rep.* **2017**, *7* (1), 3841.
(34) Lang, B. J.; et al. Heat Shock Proteins Are Essential Components in Transformation and Tumor Progression: Cancer Cell Intrinsic Pathways and Beyond. *Int. J. Mol. Sci.* **2019**, *20* (18), 4507.
(35) Zhao, K.; et al. HSP70 Family in Cancer: Signaling Mechanisms and Therapeutic Advances. *Biomolecules* **2023**, *13* (4), 601.
(36) Sha, G.; et al. The multifunction of HSP70 in cancer: Guardian or traitor to the survival of tumor cells and the next potential therapeutic target. *Int. Immunopharmacol.* **2023**, *122*, No. 110492.
(37) Halgren, T. New method for fast and accurate binding-site identification and analysis. *Chem. Biol. Drug Des.* **2007**, *69* (2), 146−8.
(38) Halgren, T. A. Identifying and Characterizing Binding Sites and Assessing Druggability. *J. Chem. Inf Model.* **2009**, *49* (2), 377−89.
(39) Kozakov, D.; Grove, L. E.; Hall, D. R.; Bohnuud, T.; Mottarella, S. E.; Luo, L.; Xia, B.; Beglov, D.; Vajda, S. The FTMap family of web servers for determining and characterizing ligand-binding hot spots of proteins. *Nat. Protoc.* **2015**, *10* (5), 733−55.
(40) Berman, H. M.; et al. The Protein Data Bank. *Nucleic Acids Res.* **2000**, *28* (1), 235−42.
(41) *Protein Data Bank, ID3B97*. Available online: https://www.rcsb.org/structure/3B97 (accessed on June 2023).
(42) Li, X.; Shao, H.; R. Taylor, I.; E. Gestwicki, J. Targeting Allosteric Control Mechanisms in Heat Shock Protein 70 (Hsp70). *Curr. Top Med. Chem.* **2016**, *16* (25), 2729.
(43) Rüdiger, S.; Buchberger, A.; Bukau, B. Interaction of Hsp70 chaperones with substrates. *Review Nat. Struct Biol.* **1997**, *4* (5), 342−9.
(44) Clerico, E. M.; Tilitsky, J. M.; Meng, W.; Gierasch, L. M. How hsp70 molecular machines interact with their substrates to mediate diverse physiological functions. *J. Mol. Biol.* **2015**, *427* (7), 1575−88.
(45) Hartl, F. U.; Bracher, A.; Hayer-Hartl, M. Molecular chaperones in protein folding and proteostasis. *Nature* **2011**, *475* (7356), 324−32.
(46) Mayer, M. P. Gymnastics of molecular chaperones. *Mol. Cell* **2010**, *39* (3), 321−31.
(47) Smock, R. G.; Blackburn, M. E.; Gierasch, L. M. Conserved, disordered C terminus of DnaK enhances cellular survival upon stress and DnaK in vitro chaperone activity. *J. Biol. Chem.* **2011**, *9;286* (36), 31821.
(48) Perovic, V.; Sumonja, N.; Marsh, L. A.; Radovanovic, S.; Vukicevic, M.; Roberts, S. G. E.; Veljkovic, N. IDPpi: Protein-Protein Interaction Analyses of Human Intrinsically Disordered Proteins. *Sci.Rep.* **2018**, *12;8* (1), 10563.
(49) Sharma, R.; Sharma, A.; Patil, A.; Tsunoda, T. Discovering MoRFs by trisecting intrinsically disordered protein sequence into terminals and middle regions. *BMC Bioinformatics* **2019**, *4;19* (Suppl 13), 378.
(50) IUPred. *IUPred Web Server*. Available online: https://iupred.elte.hu/ (accessed November 2024).
(51) Dosztányi, Z.; Mészáros, B.; Simon, I. ANCHOR: web server for predicting protein binding regions in disordered proteins. *Bioinformatics* **2009**, *15;25* (20), 2745−6.
(52) Maranto, C.; et al. Cellular stress induces cap-independent alpha-enolase/MBP-1 translation. *FEBS Lett.* **2015**, *589* (16), 2110−6.
(53) AlphaFold. *AlphaFold Protein Structure Database*. Available online: https://alphafold.ebi.ac.uk/entry/P0DMV8 (accessed November 2024).
(54) Principe, M.; et al. Targeting of surface alpha-enolase inhibits the invasiveness of pancreatic cancer cells. *Oncotarget.* **2015**, *6* (13), 11098−113.
(55) Cappello, P.; et al. Vaccination with ENO1 DNA prolongs survival of genetically engineered mice with pancreatic cancer. *Gastroenterology* **2013**, *144* (5), 1098−106.
(56) Cappello, P.; et al. Next generation immunotherapy for pancreatic cancer: DNA vaccination is seeking new combo partners. *Cancers (Basel)* **2018**, *10* (2), 51.
(57) Jung, D. W.; et al. A unique small molecule inhibitor of enolase clarifies its role in fundamental biological processes. *ACS Chem. Biol.* **2013**, *8* (6), 1271−82.
(58) Cho, H.; Um, J.; Lee, J. H.; Kim, W. H.; Kang, W. S.; Kim, S. H.; Ha, H. H.; Kim, Y. C.; Ahn, Y. K.; Jung, D. W.; Williams, D. R.; et al. ENOblock, a unique small molecule inhibitor of the non-glycolytic functions of enolase, alleviates the symptoms of type 2 diabetes. *Sci. Rep.* **2017**, *7*, 44186.
(59) Haque, A.; Capone, M.; Matzelle, D.; Cox, A.; Banik, N. L. Targeting Enolase in Reducing Secondary Damage in Acute Spinal Cord Injury in Rats. *Neurochem. Res.* **2017**, *42* (10), 2777−2787.
(60) Polcyn, R.; et al. Enolase inhibition alters metabolic hormones and inflammatory factors to promote neuroprotection in spinal cord injury. *Neurochem. Int.* **2020**, *139*, No. 104788.
(61) Zuo, J.; et al. The type 1 transmembrane glycoprotein B7-H3 interacts with the glycolytic enzyme ENO1 to promote malignancy and glycolysis in HeLa cells. *FEBS Lett.* **2018**, *592* (14), 2476−2488.
(62) Shevtsov, M.; et al. Membrane-Associated Heat Shock Proteins in Oncology: From Basic Research to New Theranostic Targets. *Cells.* **2020**, *9* (5), 1263.
(63) Zakrzewicz, D.; et al. The interaction of enolase-1 with caveolae-associated proteins regulates its subcellular localization. *Biochem. J.* **2014**, *460* (2), 295−307.

https://doi.org/10.1021/acsomega.4c10808
ACS Omega 2025, 10, 5036−5046

(64) Madhavi Sastry, G.; Adzhigirey, M.; Day, T.; Annabhimoju, R.; Sherman, W. Protein and ligand preparation: parameters, protocols, and influence on virtual screening enrichments. *J. Comput. Aided Mol. Des.* **2013**, *27* (3), 221−234.
(65) Shelley, J. C.; et al. Epik: a software program for pK(a) prediction and protonation state generation for drug-like molecules. *J. Comput. Aided Mol. Des.* **2007**, *21* (12), 681−91.
(66) Greenwood, J. R.; Calkins, D.; Sullivan, A. P.; Shelley, J. C. Towards the comprehensive, rapid, and accurate prediction of the favorable tautomeric states of drug-like molecules in aqueous solution. *Comput. Aided Mol. Des.* **2010**, *24* (6−7), 591−604.
(67) Jacobson, M. P.; Friesner, R. A.; Xiang, Z.; Honig, B. On the role of the crystal environment in determining protein side-chain conformations. *J. Mol. Biol.* **2002**, *320* (3), 597−608.
(68) Bowers, K. J.et al.*Scalable Algorithms for Molecular Dynamics Simulations on Commodity Clusters*; Proceedings of the ACM/IEEE Conference on Supercomputing (SC06) 2006.
(69) Lu, C.; et al. OPLS4: Improving Force Field Accuracy on Challenging Regimes of Chemical Space. *J. Chem. Theory Comput.* **2021**, *17* (7), 4291−4300.

https://doi.org/10.1021/acsomega.4c10808
ACS Omega 2025, 10, 5036−5046